Post-Infarction Dysregulation of Cardiac Redox Balance: Novel Avenues for Cardiovascular Disease Treatment

A thesis submitted in partial fulfillment of the requirements for the degree of Bachelor of Science with Honors in Computational Biology

Elliot Youth
Brown University
April 2020

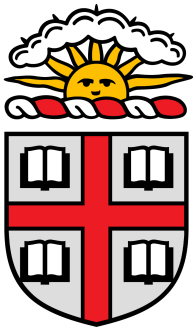

Thesis Advisor
Kareen Coulombe, PhD
School of Engineering
Center for Biomedical Engineering

Second Reader
Sorin Istrail, PhD
Department of Computer Science
Center for Computational Molecular Biology

Abstract

Myocardial infarction (MI) has profound negative effects on the cardiac microenvironment, and its long-term impacts on electrophysiologic and phenotypic alterations in the heart are of great clinical interest. Cardiac fibroblasts (CFs) are hypothesized to exert a crucial modulatory role on neighboring cardiomyocytes (CMs), such that post-MI dysregulation of critical gene pathways in CFs may compromise proper CM functioning. From transcriptomic analysis of mouse CFs, we identify glutathione-related pathways as putative drivers of redox imbalance in CFs post-MI, and pursue experiments to validate these results in human cell models.

Introduction

Cardiovascular disease (CVD) is the leading cause of mortality worldwide, responsible for nearly a third of global deaths annually.[1] Cardiac tissue engineering represents a promising field for investigation and treatment of CVD, given its utility in modeling cardiac injury for *in vitro* study and immense potential for regenerative repair of diseased hearts, and tissue scaffolds that closely mimic biological growth conditions are currently in development.[2] However, precise understanding of changes in gene expression that occur following cardiac injury remains imperative for the development of effective therapies for acutely severe heart conditions such as myocardial infarction (MI). In particular, the post-MI structural, electrophysiological, and paracrine interactions between cardiac fibroblasts (CFs) and cardiomyocytes (CMs) are not well-characterized, and represent a current area of fruitful study.

Significant differential changes have recently been documented in the hearts of mice following MI by Fu et al.[3], suggesting that transcriptomic analysis may yield insights relevant to human cardiac injuries. In particular, evidence has emerged to suggest that CFs undergo a variety of genetic and phenotypic changes following injury, and may act as critical modulators of CM function in the post-infarcted heart. These dynamic, time-dependent changes in fibroblast gene expression provide insights into the shifting transcriptomic landscape of the heart following MI, and may reveal pathways of particular relevance to not only the fibrotic scarring process, but also the development of arrhythmias. Computational analysis of public transcriptomic data from cardiac injury contexts enables elucidation of these disease-driven alterations in gene expression, and offers a method for identifying novel gene targets for assessing and combating post-MI dysfunction in the human heart.

Oxidative stress (OS) is a consequence of MI in the post-infarcted heart.[4] Rapid reperfusion of ischemic cardiac tissue is the current standard of care for clinical treatment of acute MI, but results in production of reactive oxygen species (ROS), including H_2O_2 and hydroxyl free radicals, which can damage cells and may lead to arrhythmogenesis by compromising redox balance.[5–7] Glutathione, a tripeptide with a reducing sulfhydryl moiety, is the main antioxidant in the human heart, and plays critically important roles in maintaining intracellular redox balance and protecting cells from exogenous toxins and reactive endogenous compounds which are generated in the OS response.[8,9] Its synthesis, conjugation to reactive compounds, and degradation are crucial to intracellular redox balance as well as to core fibroblast mechanisms including proliferation and apoptosis.[9–12] In healthy cells, the ratio of reduced glutathione molecules (GSH) to oxidized glutathione dimers (GSSG) is on the order of 100:1; this ratio falls to 1:10 under OS conditions.[8] Numerous studies have reported an inverse relationship between endogenous GSH levels and severity of various CVD phenotypes, including MI and arrhythmia.[13–16]

Glutathione-related pathways involve controlled regulation of dozens of genes responsible for the important processes of synthesis and conjugation. Glutathione-S-transferases (GSTs) are drivers of glutathione metabolic processes, in particular through conjugation of glutathione to reactive secondary metabolites produced by ROS-inflicted oxidative degradation of intracellular biomolecules, and their expression is typically upregulated upon induction of OS and antioxidant activity.[17–19] Thus, GSTs are crucial to glutathione-mediated protection against the effects of reperfusion-induced ROS generation, and represent a potential therapeutic target for combating OS-driven pathology in the post-MI heart.

Here, bioinformatic analysis of transcriptomic data published by Fu et al.[3] was undertaken to identify dysregulated gene pathways to guide experimental study and inform development of therapeutics for MI.

Methods

Acquisition of data. Original data published by Fu et al. was obtained from the NCBI Gene Expression Omnibus (GEO) database (accession GSE111059).[3] Data comprised 14 raw microarray fluorescence intensity readings of 50,000 *Tcf21* lineage-traced CFs isolated from uninjured mice and mice at multiple timepoints following MI induced through permanent ligation of the left coronary artery (complete methods detailed in Fu et al.[3]). Raw data was processed using the `clariomsmousetranscriptcluster.db` and `oligo` packages in R (version 3.6.1).[20–22]

Quality control of Fu et al. microarray data. Raw fluorescence intensities for 29,129 genes were processed prior to analysis as follows. All expression levels were normalized using the Robust Multichip Average (RMA) quantile method to enable direct comparison of gene expression across samples. Lowly-expressed transcripts exhibiting background intensity levels were filtered out by setting a threshold at a median $\log_2$-intensity of 5.5 and retaining only transcripts which exceeded this threshold in at least 2 samples (corresponding to the smallest number of biological replicates across any timepoint). Following reduction and filtering of the normalized median intensities from a bimodal to a unimodal distribution, transcript annotations were synchronized between the native microarray probelist (Affymetrix Clariom S Assay, Mouse) and Official Gene Symbol IDs, using the `AnnotationDbi` package in R, to enable downstream interpretation and gene pathway analysis.[23] Final quality-controlled data comprised normalized, filtered and annotated fluorescence intensity readings for 15,714 genes across 14 CF samples. See Supplementary Figures for detailed quality control workflow (Figure S1).

Identification of differentially-expressed genes. Empirical Bayesian methods employing moderated t-statistics computed on a genewise basis were used to assay for differential expression of specific genes at individual timepoints post-MI relative to the uninjured baseline, using the `limma` package in R.[24] Differentially-expressed genes (DEGs) were identified using a threshold of FDR < 0.05, with raw p-values corrected using the Benjamini-Hochberg (BH) method. Any gene differentially-expressed at one or more timepoints post-MI was included in a final list of DEGs for downstream analysis.

Analysis and visualization of computational results. Graphical visualizations of DEG analysis results were produced from quality-controlled data. Heatmaps, Venn diagrams and boxplots/barplots were generated with the `gplots`, `VennDiagram`, and `ggplot2` packages in R, respectively.[25–27]

Gene ontology (GO) analysis. DEGs were sorted into numerous subgroups based on timepoint(s) at which dysregulation was exhibited and directionality of differential expression (i.e., upregulated/UR or downregulated/DR). Curated DEG lists were then imported into the PANTHER (protein analysis through evolutionary relationships) database for clustering by PANTHER and Reactome pathways and identification of subsets of genes to guide further investigation.[28,29] Significant dysregulation of individual pathways was inferred using the Statistical overrepresentation test tool applied to lists of directionally-segregated DEGs at specific timepoints post-MI. General pathway dysregulation was assessed using the Functional classification viewed in graphic charts tool.

Cell culture. Primary human cardiac fibroblasts (hCFs) were obtained from Sigma-Aldrich (product #306-05F). Cells were subcultured in a custom hCF media composed of Dulbecco's Modified Eagle Medium/Nutrient Mixture F-12 (DMEM/F-12) from Gibco (cat. no.: 11320033) supplemented with 10% fetal bovine serum (FBS) and 1% Penicillin-Streptomycin (Pen-Strep) from Sigma-Aldrich (products #F4135, #P0781). Upon seeding, cells were additionally treated with 4 ng/ml basic fibroblast growth factor (bFGF) from ReproCELL (code: 03-0002). Cells were subcultured to confluence in 100 mm dishes up to passage 10 (P10) for toxicity testing and redox imbalance experiments.

Toxicity testing. P6 hCFs were subcultured in 96-well plates for triplicate exposure to simulated ischemia-reperfusion (I-R) and oxidative stress (OS). I-R was simulated by introducing cells into a closed hypoxic chamber with oxygen levels maintained at 3% O_2, immediately replacing existing media with media that had been warmed and de-oxygenated within the chamber for a minimum of two hours prior, allowing cells to incubate for a period of time (ranging from 30 minutes to 24 hours), and subsequently restoring cells to normoxic conditions (21% O_2) to mimic reperfusion. Simulated OS was

induced by supplementing existing media with varying concentrations of H_2O_2 for 4 hours, after which normal hCF media was restored. Following exposure to hypoxia or H_2O_2, cells were assayed to assess toxicity of each experimental condition. Cell viability and cytotoxicity were assayed using the CyQUANT™ MTT Cell Viability Assay and Pierce™ LDH Cytotoxicity Assay Kit, both from Thermo Fisher Scientific (cat. nos.: V13154, 88953). MTT and LDH assay activities were quantified by colorimetric plate reader. All colorimetric readings were conducted in colorless Tyrode's solution.

Assessment of redox imbalance. P10 hCFs were subcultured in 50 mm FluoroDishes for exposure to hypoxia (3% O_2), ROS (50 μM H_2O_2), and high glucose (30 mM D-glucose). Hypoxia was induced as described above; H_2O_2 and D-glucose were supplemented to normal hCF media at the indicated concentrations. After 24 hours of exposure, cells were restored to normal hCF media and normoxic conditions, and stained with both MitoSOX™ Red Mitochondrial Superoxide Indicator and Wheat Germ Agglutinin Alexa Fluor™ 488 conjugate (WGA) from Invitrogen (cat. nos.: M36008, W11261). After 10 minutes, cells were washed thrice with PBS and mounted in Tyrode's solution for live-cell confocal imaging. Superoxide (O_2^-) activity was employed as a proxy for redox imbalance, and quantified as the mean intracellular MitoSOX fluorescence intensity (excluding WGA background signal) from confocal images using ImageJ (version 1.52).[30]

Analysis and visualization of experimental results. Statistical analysis of experimental data was conducted in Microsoft Excel. One-way unpaired heteroscedastic t-tests were employed to test for significant differences between treatment groups.

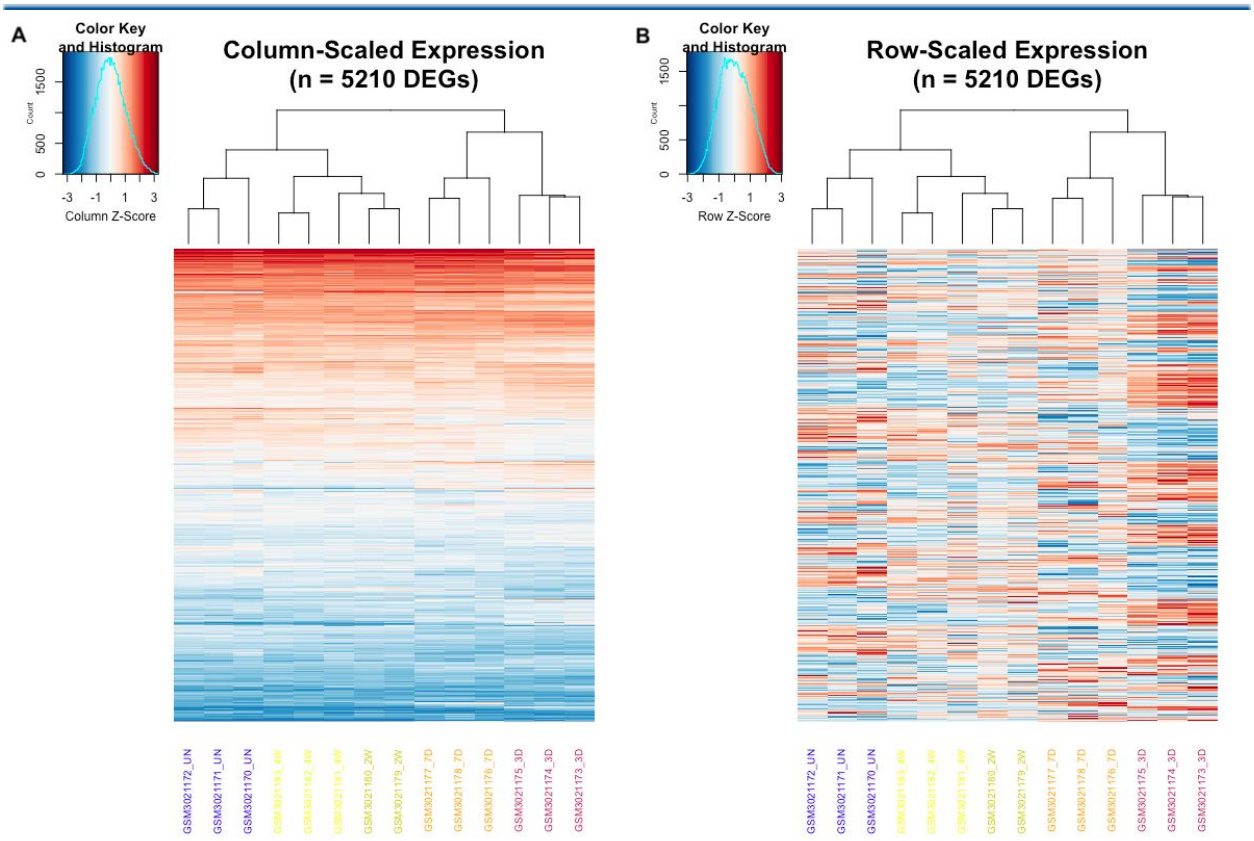

Figure 1. Differential gene expression varies across the timecourse. (**A**) Sample-normalized expression values for 5,210 DEGs across 14 mouse CF samples from Fu et al.[3] (**B**) Gene-normalized expression values for the same. (**A**–**B**): Red/blue coloration indicates high/low relative expression, respectively. Sample ID timepoint annotations: UN = uninjured; 3D/7D/2W/4W = 3 days/7 days/2 weeks/4 weeks post-MI. Genes and samples are ordered identically in both plots. Dendrograms represent unsupervised clustering of samples based on expression across all DEGs.

Results

Disparate patterns of dysregulated gene expression manifest across the post-MI timecourse. Heatmap clustering of all samples by relative expression of all DEGs reveals substantial variation in expression levels, both between individual post-MI timepoints and the uninjured baseline as well as between multiple disparate post-MI timepoints. Red-blue gradient visualization of sample-normalized data (Figure 1A) suggests that multiple distinct clusters of lowly-expressed and highly-expressed genes are significantly dysregulated following MI, while visualization of gene-normalized data (Figure 1B) localizes the most severe dysregulation (represented by greater red/blue color intensity) to the samples obtained at 3 days following MI ("GSM#_3D"). Unsupervised sample clustering places acute-phase timepoints (3D/7D) and uninjured/chronic-phase timepoints (UN, 2W/4W) into distinct subgroups (Figure 1), suggesting that immediate response to injury results in substantial gene dysregulation relative to the uninjured baseline, which is gradually attenuated over the extended post-MI timecourse.

DEGs identified across the post-MI timecourse yield distinct subgroups of future interest. Principal component analysis of samples based on expression of all DEGs (Figure 2A) concurs with dendrograms in Figure 1, suggesting that severe injury status vs. uninjured or recovering injury status is the primary source of inter-sample variation (PC1) while earlier vs. later timepoint is the secondary source of variation (PC2). Of interest, the two latest post-MI timepoints (2W, 4W) are clustered relatively closely together, suggesting the development of a stable chronic phenotype (dubbed the *matrifibrocyte* by Fu et al.[3]) whose expression profile differs significantly from that of the acute phase. This discrepancy between early and late timepoints is corroborated by the overlapping quantification of all 5,210 DEGs across the entire timecourse (Figure 2B), which identifies 4,213 DEGs (>80% of total) significantly dysregulated only in the acute phase (3D, 7D) and 2,284 DEGs (>40% of total) dysregulated solely at the 3D post-MI timepoint. 211 genes (4% of the total) were found to become significantly dysregulated only after at least 2 weeks following MI, while 44 of these (<1% of total) were significantly dysregulated at both 2 weeks and 4 weeks following MI. The central group of 260 DEGs (5% of total) which were significantly dysregulated at all timepoints post-MI are of particular interest, as they may contribute to both short- and long-term injury by driving changes in phenotype. These subsets of DEGs were further investigated to identify timepoint-specific patterns.

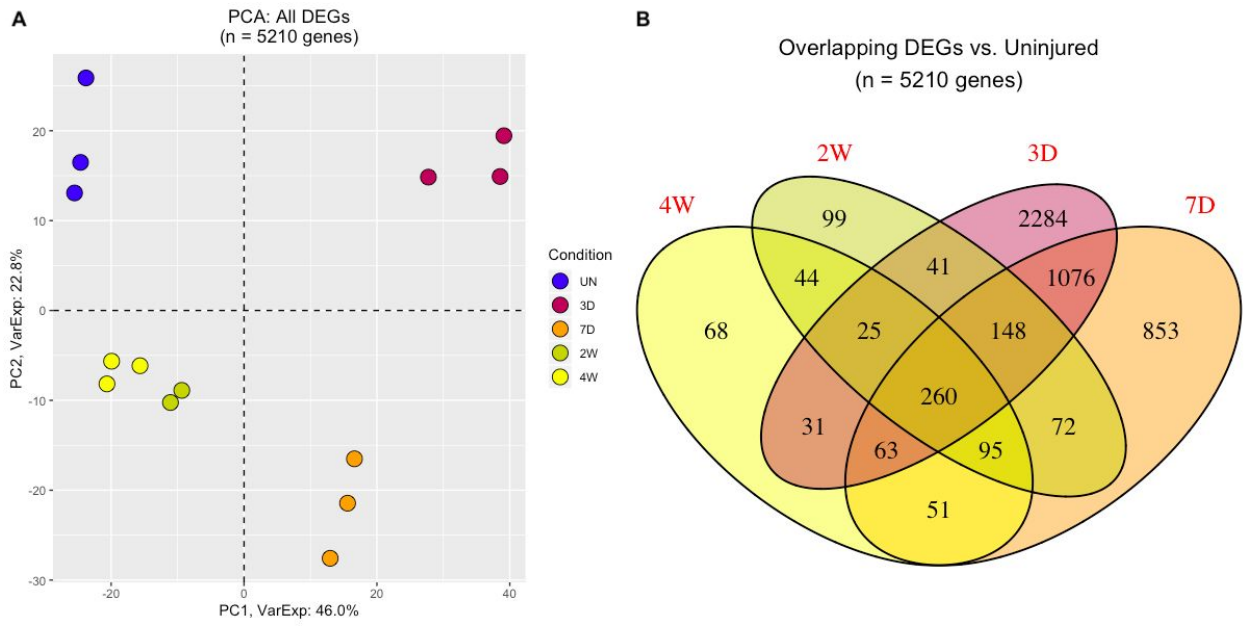

Figure 2. Distinct DEGs characterize acute and chronic phases post-MI. (**A**) Principal component analysis of samples based on expression across all DEGs. (**B**) Number of DEGs identified in each subset of timepoints post-MI.

Reactome Pathway	FDR
Extracellular matrix organization	6.09×10^{-8}
Elastic fibre formation	8.95×10^{-5}
Non-integrin membrane-ECM interactions	2.28×10^{-3}
Integrin cell surface interactions	2.69×10^{-3}
Molecules associated with elastic fibres	2.75×10^{-3}
Collagen formation	5.29×10^{-3}
ECM proteoglycans	5.91×10^{-3}
Signaling by Receptor Tyrosine Kinases	1.40×10^{-2}
Biological oxidations	1.80×10^{-2}
Glutathione conjugation	2.82×10^{-2}
Crosslinking of collagen fibrils	3.85×10^{-2}
Cell surface interactions at the vascular wall	4.34×10^{-2}
Hemostasis	4.59×10^{-2}

Table 1. Fibroblast- and oxidation-related pathways are preferentially dysregulated across the full post-MI timecourse. All 13 significantly-overrepresented (FDR < 0.05) Reactome pathways in the list of 260 DEGs dysregulated at all timepoints post-MI. Inclusion in this list is agnostic with respect to directionality of dysregulation (UR/DR) of component genes at individual timepoints. Pathways implicated in structural and/or extracellular functions generally associated with activated fibroblasts are italicized; those implicated in intracellular functions associated with redox balance are bolded.

Persistently-dysregulated genes are predominantly associated with structural and connective functions. Thirteen Reactome pathways were identified as significantly overrepresented (FDR < 0.05) in the list of 260 DEGs dysregulated across the entire post-MI timecourse (Table 1). The majority of these pathways appear to play structural or intercellular connectivity roles, as expected based upon the activating changes in CF phenotype described by Fu et al. in their initial analysis.[3] Investigation of all such genes annotated with the ontology label Biological Process: Biological Adhesion corroborated this inference, revealing substantial short- and long-term upregulation of several cadherins (*CDH2*, *CDH3*) in addition to other genes involved in fibroblast activation (*FN1*, *POSTN*) (Figure S2).

Acutely- and chronically-upregulated pathways exhibit a gradual return to baseline expression levels. The majority of 3D-only and 2W/4W-only DEGs were significantly upregulated. The "acute" DEG set featured numerous genes involved in inflammation and immediate response to wounding (Figure S3A), while the corresponding "chronic" DEG set featured many fewer such genes overall, with a greater focus on fibroblast growth (Figure S3B).

Numerous ion channel genes exhibit sustained dysregulation following MI. Several genes annotated with the ontology label Molecular Function: Ion Transmembrane Transporter Activity became chronically-dysregulated throughout the post-MI timecourse. Among the chronically-upregulated set were several Ca^{2+} (*CACNA1C*, *CACNA1G*) and K^+ (*ERG*, *KCNE4*, *KCNJ15*, *KCNMA1*) channel genes, as well as the mechanosensitive ion channel *PIEZO2* (Figures S4A, B). Chronically-downregulated genes included several K^+ channel genes (*KCNG4*, *KCNK2*) among others (Figures S4C, D).

Glutathione-related pathways are singularly downregulated across the post-MI timecourse. Comparatively few gene pathways were significantly overrepresented in lists of downregulated DEGs from specific timepoints post-MI. Reactome biological oxidation and conjugation annotations were the sole such pathways found to be significant (FDR < 0.05) at any of the timepoints (Table 2). The phenomenon of both acute and chronic downregulation of multiple genes (45 total) involved in these pathways suggests a mechanism for long-term dysregulation of cellular processes, as glutathione metabolism is crucial to maintenance of intracellular redox balance.

Table 2. Glutathione- and oxidation-related pathways are preferentially downregulated across the full post-MI timecourse. All 3 significantly-overrepresented (FDR < 0.05) Reactome pathways in the lists of DEGs downregulated at each timepoint post-MI. Forty-five unique genes were identified in all.

DEG list	Reactome Pathway	# Genes	FDR
3D DR	Biological oxidations	36	4.41×10^{-2}
7D DR	Biological oxidations	33	7.16×10^{-3}
2W DR	Glutathione conjugation	11	5.19×10^{-7}
	Biological oxidations	18	2.76×10^{-5}
	Conjugation of compounds	11	2.94×10^{-4}
4W DR	Biological oxidations	13	2.55×10^{-2}

Figure 3. Numerous glutathione-related genes are primarily downregulated across the post-MI timecourse. (**A**) Log_2-expression of glutathione metabolism DEGs across all conditions. (**B**) Log_2-fold changes in expression for glutathione metabolism DEGs across all post-MI timepoints, relative to uninjured baseline. (**C**) Log_2-expression of glutathione transferase DEGs across all conditions. (**D**) Log_2-fold changes in expression for glutathione transferase DEGs across all post-MI timepoints, relative to uninjured baseline. (**A**), (**C**): Dotted red lines indicate median intensity threshold used to filter lowly-expressed probes (Figure S1). (**B**), (**D**): *p<0.05, **p<0.01, ***p<0.001, ****p<0.0001.

Crucial glutathione-related genes are significantly dysregulated following MI. Multiple genes annotated with the ontology label Biological Process: Glutathione Metabolic Process were found to be significantly dysregulated throughout the post-MI timecourse, including both subunits of the catalytic enzyme responsible for glutathione synthesis (*GCLC*, *GCLM*), the enzyme responsible for reduction of oxidized glutathione (*GSR*), and several glutathione S-transferases (Figures 3A, B). Many genes (GSTs) annotated with the ontology label Molecular Function: Glutathione Transferase Activity were found to be exclusively downregulated following MI, with several exhibiting sharply-decreased expression in the acute-injury phase and prolonged reduced expression throughout the rest of the post-MI timecourse (Figures 3C, D). As the majority of these DEGs are members of the chronically-downregulated Reactome pathways listed in Table 2, several genes related to synthesis, reduction and conjugation of glutathione were selected for further experimental study in human cell models of MI/OS (Figure S5).

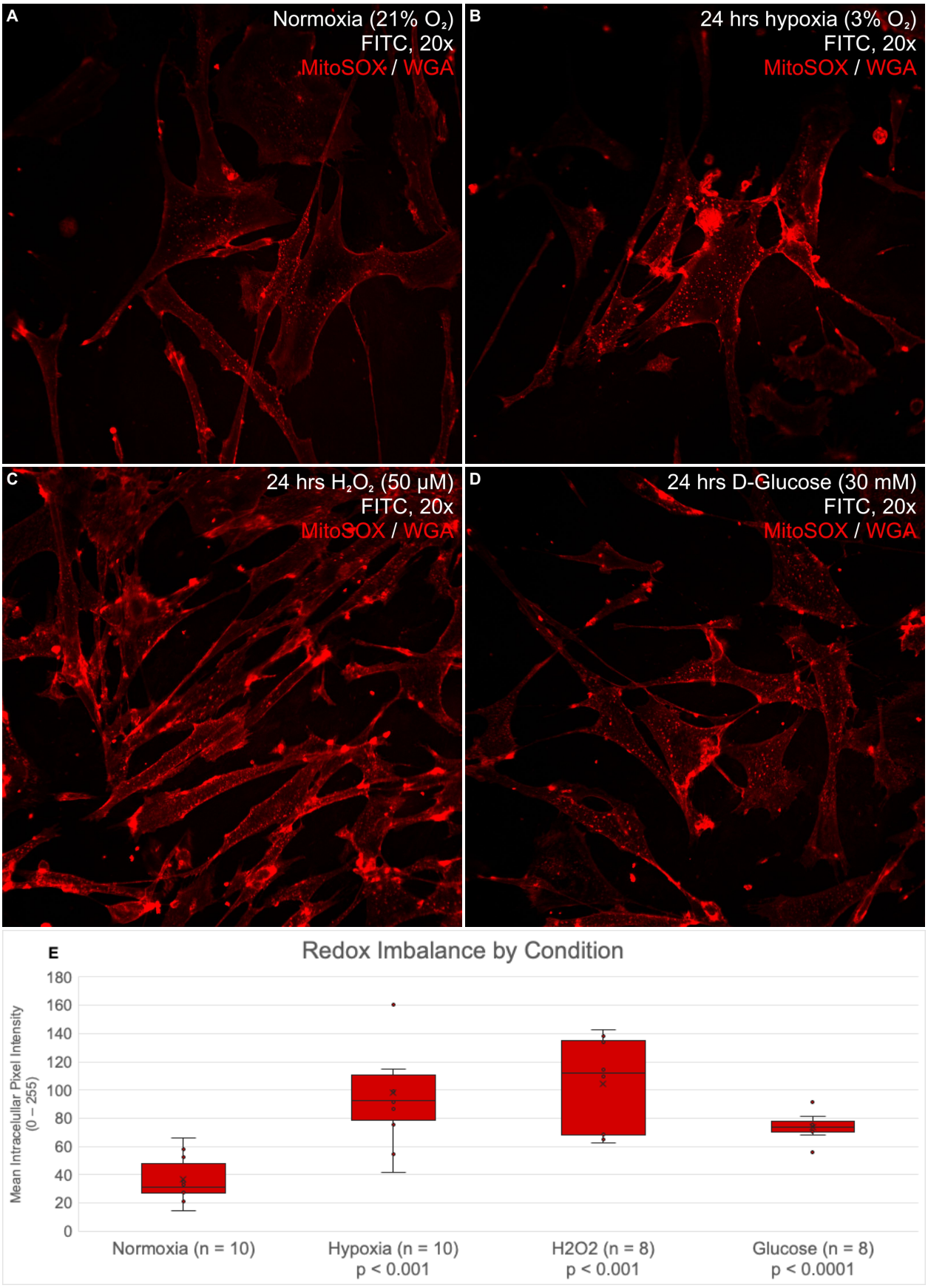
A
Normoxia (21% O_2)
FITC, 20x
MitoSOX / WGA
B
24 hrs hypoxia (3% O_2)
FITC, 20x
MitoSOX / WGA
C
24 hrs H_2O_2 (50 µM)
FITC, 20x
MitoSOX / WGA
D
24 hrs D-Glucose (30 mM)
FITC, 20x
MitoSOX / WGA
E
Redox Imbalance by Condition
Mean Intracelullar Pixel Intensity (0 – 255)
180
160
140
120
100
80
60
40
20
0
Normoxia (n = 10)
Hypoxia (n = 10)
p < 0.001
H2O2 (n = 8)
p < 0.001
Glucose (n = 8)
p < 0.0001

Figure 4. Experimental induction of I-R and OS in hCFs activates ROS production. (**A**–**D**) Representative live-cell 20x confocal images of P10 hCFs following various treatments: (**A**) hCFs incubated in standard normoxic conditions (21% O_2); (**B**) hCFs incubated for 24 hours in hypoxic conditions (3% O_2) to simulate I-R; (**C**) hCFs treated with H_2O_2 (50 μM) to simulate OS; (**D**) hCFs treated with D-glucose (30 mM). (**E**) Quantification of redox imbalance via superoxide (O_2^-) activity as measured by mean intracellular MitoSOX fluorescence intensity (n = # cells quantified per condition). Boxplots indicate means (x), medians and IQRs. One-way unpaired t-tests for unequal variance were computed relative to the control (normoxia) distribution to yield the p-values shown for each experimental condition.

Experimental simulation of I-R and OS induces redox imbalance in hCFs. Following toxicity testing, 24 hours of hypoxia exposure was judged sufficient to induce OS in hCF models of MI (Figures S6A, B), while 50 μM H_2O_2 was deemed an optimal concentration to induce cellular stress without substantial cell death (Figures S6C, D). Increased presence of mitochondrial ROS was observed in all experimental models of I-R and OS, based on fluorescence intensity of MitoSOX superoxide (O_2^-) indicator. Qualitatively, the spatial concentration and intensity of intracellular punctae was increased in hCFs exposed to hypoxia (Figure 4B) or treated with H_2O_2 (Figure 4C) or high levels of glucose (Figure 4D), relative to hCFs which were maintained under normoxic conditions (Figure 4A). Quantification of mean intracellular MitoSOX signal from live-cell confocal images revealed significant increases for all three experimental conditions, suggesting the utility of these hCF models for simulating I-R and OS responses to probe the aftereffects of MI *in vitro*.

Discussion

The computational results of this study largely concur with the findings reported by Fu et al.[3], validating the bioinformatics pipeline employed for analysis and subsequent inference of genetic changes exhibited by mouse CFs following surgically-induced MI. In particular, several key findings were generally replicated by this analysis: 1) approximately 5,000 total DEGs were identified across the post-MI timecourse, the majority of which were dysregulated solely in the acute phase (Figures 1, 2B); 2) distinct clusters of highly- and lowly-expressed DEGs were found (Figure 1A); 3) expression-based clustering segregated 3D/7D CFs from UN/2W/4W CFs (Figures 1B, 2A); and 4) numerous genes critical to fibroblast evolution and structural development pathways were found to be significantly upregulated in both the acute and chronic phase post-MI (Table 1; Figure S2). These broad-scale shifts in patterns of gene expression and pathway activation provide computational evidence to support existing models of cardiac pathology, suggesting that quiescent CFs undergo a progressive evolutionary trajectory following MI and may exert significant dysregulatory impact upon the post-infarcted cardiac tissue microenvironment, with potential implications for phenotypic and electrophysiological dysfunction of neighboring CMs over a longer timescale.

GO analysis of the DEG lists identified across the post-MI timecourse yields additional insights into specific pathways which appear to be preferentially dysregulated following injury. Gene sets which were dysregulated solely in the acute phase (3D) post-MI featured significant upregulation of various pathways involved in the cellular injury response, including inflammatory signaling and proteasome activity (Figure S3A). Conversely, the population of DEGs which emerged as dysregulated later in the post-MI timecourse featured several genes involved in long-term fibroblast remodeling, including pathways related to intercellular connectivity, fibrotic scarring and development of the matrifibrocyte phenotype characterized by Fu et al.[3] (Table 1; Figure S3B). Numerous and diverse ion transmembrane transport genes were identified as chronically-sustained DEGs (Figure S4), suggesting that electrophysiological mechanisms and intracellular ion balance may indeed be detrimentally impacted by MI. These findings provide further support for the hypothesis that CFs play a crucial role in modulating cardiac dynamics following injury, as evidenced by the substantial genetic and phenotypic changes they undergo throughout the wound healing and scarring process.

While the subsets of DEGs identified as upregulated across the post-MI timecourse suggest mechanisms of positive dysfunction which likely contribute to long-term changes in phenotype, the balance of downregulated DEGs indicate possible

pathways of negative dysfunction which merit further study. In particular, the significant downregulation of numerous genes related to biological oxidation and glutathione conjugation pathways across the entire post-MI timecourse (Table 2; Figures 3, S5) implicate redox imbalance as a possible driver of long-term cardiac dysfunction in the post-infarcted heart, and inspired the experimental phase of this study, which focused on developing human cell models of MI to validate these bioinformatic findings in a more clinically-relevant context.

The physiological fidelity of *in vitro* models of MI is of paramount importance in order to ensure that results are applicable to human disease *in vivo*. In particular, the ability of experimental treatments to adequately stress cells without exhibiting significant cytotoxicity was a primary concern of this study. Various clinical guidelines recommend percutaneous reperfusion of ischemic cardiac tissue within 90–120 minutes following onset of MI in order to minimize long-term damage to the heart, as significant death of myocardial cells can occur in as few as 4 hours.[4,6,31–33] Prior experimental models have simulated ischemia through short-term exposure to O_2-deficient cell environments or media, with exposure times ranging from 1 to 24 hours; some studies have reported robust survival of mouse CMs for up to 6 hours of exposure to hypoxia.[34,35] The hypoxia model tested here, involving varied durations of exposure to a 3% O_2 environment, revealed moderately-decreased cell viability and minimally-increased cytotoxicity across an extended range of time (Figures S6A, B). Given the resilience of hCFs when cultured under such conditions, 24 hours was selected as an appropriate length of time for modelling I-R-induced OS. Based on both qualitative and quantitative assessments, the hypoxia model was sufficient to induce increased ROS generation relative to cells maintained under normoxic conditions (Figures 4A, B, E).

ROS are a hallmark of I-R-induced OS, and many experimental models for MI have involved direct application of H_2O_2 to both rat and mouse CFs/CMs, at concentrations ranging from 25 μM to 100 μM.[34–37] As cell viability has been reportedly reduced within as few as 6 hours of exposure to H_2O_2, various concentrations were tested here over exposures of 4 hours, suggesting that 50 μM H_2O_2 was sufficient to induce moderate suppression of cell proliferation with minimal cytotoxicity (Figures S6C, D). Here, simulated OS was maintained for 24 hours in order to assess ROS production alongside hypoxia exposure of the same duration. Similar qualitative and quantitative results were observed, demonstrating significant induction of ROS generation relative to normoxic controls (Figures 4A, C, E).

Exposure to high levels of glucose has also been reported as a driver of OS, with 30 mM D-glucose having been shown to induce production of ROS in human coronary artery cells.[38] Here, when exposed to the same concentration of D-glucose for 24 hours, hCFs exhibited a similarly-significant increase in ROS generation relative to cells whose normal media was not supplemented with additional glucose (Figures 4A, D, E). These results validate an alternative method of inducing OS for *in vitro* study of post-MI changes in cardiac gene expression.

Although hypoxia, H_2O_2 and high glucose all induced significant ROS generation in hCFs after 24 hours, the magnitude and reliability of this effect varied between experimental conditions. Based on quantitative analysis of confocal images (Figures 4A–D), high glucose resulted in a ≈2-fold increase in median intracellular MitoSOX signal, while increases in median intensity of ≈3–4x were observed across cells treated with hypoxia and H_2O_2 (Figure 4E). These differences are reflected qualitatively in the representative images shown here, which reveal generally-increased frequency and intensity of intracellular punctae indicative of mitochondrial superoxide activity under the latter two conditions (Figures 4B, C). Mean fluorescence intensities of the cells exposed to either hypoxia or H_2O_2 exhibited a greater spread overall compared to those of the control cells or cells treated with high glucose; however, this variability was likely an artifact due to the small number of cells analyzed here, and should not overshadow the significant increase in MitoSOX signal observed under both experimental conditions. These increases also concur with previous reports of 3–6-fold changes in fluorescence intensity following induction of OS in both rat and human cardiac cells[38], validating both the hypoxia and H_2O_2 treatments employed here as *in vitro* models for experimental study of MI in hCFs. The shared cardiac micro-environment suggests the applicability of simulated treatments to the study of human CMs as well.

The findings presented here regarding post-MI gene dysregulation in mouse CFs are illuminating, but require validation in human cell models of MI in order to inform development of clinical therapeutics. Of particular interest are the broad downregulation of glutathione-related pathway genes observed across the post-MI timecourse as well as the significant induction of ROS generation demonstrated in various experimental hCF models of MI (Figures 3, 4). Further experiments focused on probing the post-MI dynamics of genes involved in glutathione-related pathways in human CFs and CMs may yield actionable insights into potential paracrine mechanisms of cellular dysfunction and development of pathological cardiac phenotypes.

Among the 45 total DEGs comprising the few significantly-downregulated Reactome pathways in the post-MI mouse CFs (Table 2) were numerous genes involved in glutathione metabolism and conjugation (Figure 3). From these cohorts, specific glutathione-related DEGs of further interest were identified (Figure S5): *GCLC* and *GCLM* (catalytic and modifier subunits of glutamate-cysteine ligase, the rate-limiting enzyme in glutathione synthesis); *GSR* and *GPX3* (genes responsible for reduction of GSSG and H_2O_2, respectively); and GSTs *GSTA3*, *GSTK1*, *GSTM1* and *GSTT1*. These 8 genes were selected for their central roles in glutathione homeostasis as well as their representative patterns of dysregulation across the post-MI timecourse: *GCLC* and *GCLM* both appeared to fluctuate significantly in the acute phase (3D/7D) following MI; *GPX3* and *GSR* exhibited opposite trends of directional dysregulation, with unknown effects upon cellular levels of GSH and ROS; and the 4 GSTs selected here all underwent acute decreases in expression followed by gradual restoration towards uninjured baseline levels (Figure S5).

Having identified these glutathione-related genes of interest in mouse models, a logical next step will be to conduct experimental investigation of their timecourse dynamics in human cell models of MI. Validation of similar effects in human CFs and CMs will enable further study of the relationship between glutathione-related pathway dysfunction and chronic redox imbalance as a potential driver of post-MI OS and subsequent cardiac injury, paving the way for development of clinical therapies.

Future Directions

Proposed methodologies and anticipated outcomes of future experiments are detailed below.*

(1) Robust confirmation of utility of experimental treatments for simulating the effects of MI in hCFs. The experimental induction of I-R and OS in hCF models as detailed here will be replicated and quantified in a greater number of cells in order to confirm the validity of these models for reliably simulating MI *in vitro*. MitoSOX fluorescence intensity assessed by flow cytometry will enable precise quantification of mitochondrial superoxide activity and confirm significant generation of ROS in response to induced I-R or OS.[38] Assessment of ROS in lower-passage hCFs or at lower O_2 levels could also provide more definitive evidence for the robust induction of ROS generation under hypoxic or oxidatively-stressed conditions, relative to normoxic controls. Larger-scale quantification of cells will likely decrease the variability in MitoSOX signal observed in cells exposed to hypoxia and H_2O_2, and establish whether one model may be better-suited for inducing significant ROS in future experiments.

(2) Validation of post-MI glutathione-related pathway dysfunction in hCFs. Once the hCF models of MI presented here are shown to be robust, the crucial glutathione-related genes identified here will be assessed for similar patterns of downregulated expression as observed in mouse models of MI. Following exposure of hCFs to either simulated I-R (via incubation in hypoxic conditions for 24 hours) or simulated OS (via direct treatment with H_2O_2), RNA extraction and transcriptomic quantification via RT-qPCR will reveal the extent to which the 8 glutathione-related genes of interest are significantly downregulated in the "post-MI" cells compared to normoxic, untreated controls. The transcription factor *HIF1A* will be employed as a positive control, as its expression is activated following ischemia-induced hypoxia.[5,39] 18S rRNA will serve as a housekeeping control. Results will establish whether similar patterns of glutathione pathway dysregulation are induced in hCFs post-MI. If broad downregulation of these 8 genes is observed as hypothesized, further experiments may be conducted to elucidate the potential impacts of CF dysregulation on ROS generation and CM gene expression following MI, bringing the model into greater clinical relevance.

(3) Investigation of post-MI crosstalk between human cardiac fibroblasts and cardiomyocytes. Following validation of glutathione-related pathway dysregulation in hCFs, the scope of study will be expanded to examine the influence of such changes on human CMs. In the heart, CFs and CMs are physiologically linked through both physical proximity and paracrine signaling, and ROS are known to exert paracrine effects by diffusing into nearby cells to regulate physiological function and OS.[40,41] Thus, downregulation of genes involved in glutathione metabolism in hCFs following MI may contribute to inducing OS in neighboring CMs through dysregulation of redox balance activity. Cardiomyocytes derived from human iPS cells (hCMs) will be cultured under both normoxic and induced I-R/OS conditions in order to assess hCM-specific responses to simulated MI, in a manner akin to that described for hCFs in (1) and (2) above. Subsequently, hCMs will be cultured in transwells to examine the paracrine effects of hCFs in the post-MI context. Co-cultures of hCFs and hCMs will be established in transwells to enable paracrine communication and diffusion of metabolites between cell types while maintaining physical separation, in order to mimic intercellular crosstalk in the cardiac microenvironment.[42–44] Post-MI expression of the aforementioned genes of interest will be assessed via RT-qPCR in experimental cell populations composed of hCMs isolated from transwell co-cultures with hCFs, relative to control cell populations composed solely of hCMs. The effects of direct induction of OS via application of nonlethal concentrations of H_2O_2 may alternatively be examined in order to corroborate or supplement results from the simulated I-R context. Redox balance in oxidatively-stressed cells will be assessed via colorimetric assays for GSH and ROS concentration. The results of these experiments will enable characterization of any immediate effects on redox balance pathways following induction of simulated MI in isolated cultures of hCMs, as well as establish whether the added presence of hCFs in physically separated co-cultures confers any indirect effects on glutathione-related pathway dysregulation in hCMs through paracrine interactions. In particular, this experiment will probe whether the dysregulation of various redox balance pathways which occurs in hCFs following MI induces, exacerbates or interferes with the OS response in neighboring hCMs. Finally, insights into the influence of hCFs on OS-triggered metabolic shifts in hCMs may implicate ROS generation as a proximal driver of chronic post-MI injury in the heart and offer avenues for proactive treatment to combat secondary cardiac injury.

(4) Translational experimentation for development of therapeutics. Establishment of a modulatory role for CFs on CMs in human cell models of MI would suggest mechanisms for arrhythmogenesis, chronic ischemia and cardiac remodeling following injury, as well as therapeutic targets for combating cardiac redox imbalance in CVD patients. If post-MI glutathione-related pathway dysregulation in hCFs and subsequent induction of pathology in hCMs is observed, further experiments to assess therapeutic utility of various interventions will be devised. For example, patch-clamp or optical mapping methods may be employed to investigate whether post-MI OS induces arrhythmogenic electrophysiology in hCMs when co-cultured with hCFs. If broad downregulation of the 8 glutathione-related genes (in particular the 4 GSTs) is observed, overexpression studies in hCFs may be undertaken to determine whether restoration of baseline expression levels of glutathione-related pathway genes attenuates OS-driven dysfunction in hCFs and neighboring hCMs. Finally, live-cell FACS of mixed co-cultures would enable cell type-specific analysis in models with greater physiological fidelity. The ultimate goal of these studies will be to validate glutathione-related pathway dysfunction as a driver of negative phenotypic changes in hCFs and hCMs following MI, and translate these findings to develop novel clinical therapies for CVD (Figure S7).

Acknowledgements

A debt of gratitude is owed to KC, whose support was crucial to this thesis, as well as to the rest of the Coulombe Lab; in particular, FM, CK, RK, AM, KD, CP, AA, AS, and JR, for guidance and assistance with the experimental phase of this project. Valued consultation was provided by UM, BC, JW, and EA. XF and JM provided the public gene expression data which fueled this investigative study. This thesis was partially supported by funding from the Research at Brown Grant, generously provided by RAB.

* Temporary closure of Brown University in March 2020 due to the COVID-19 pandemic precluded further experimental work, which will be carried out by members of the Coulombe Lab following resumption of research activities.

References

1. World Health Organization. Cardiovascular diseases (CVDs). https://www.who.int/news-room/fact-sheets/detail/cardiovascular-diseases-(cvds) (2017).
2. Munarin, F., Kaiser, N. J., Kim, T. Y., Choi, B.-R. & Coulombe, K. L. K. Laser-Etched Designs for Molding Hydrogel-Based Engineered Tissues. *Tissue Eng. Part C Methods* **23**, 311–321 (2017).
3. Fu, X. *et al.* Specialized fibroblast differentiated states underlie scar formation in the infarcted mouse heart. *J. Clin. Invest.* **128**, 2127–2143.
4. McDougal, A. D. & Dewey, C. F. Modeling oxygen requirements in ischemic cardiomyocytes. *J. Biol. Chem.* **292**, 11760–11776 (2017).
5. Shohet, R. V. & Garcia, J. A. Keeping the engine primed: HIF factors as key regulators of cardiac metabolism and angiogenesis during ischemia. *J. Mol. Med. Berl. Ger.* **85**, 1309–1315 (2007).
6. O'Gara Patrick T. *et al.* 2013 ACCF/AHA Guideline for the Management of ST-Elevation Myocardial Infarction: Executive Summary. *Circulation* **127**, 529–555 (2013).
7. González-Montero, J., Brito, R., Gajardo, A. I. & Rodrigo, R. Myocardial reperfusion injury and oxidative stress: Therapeutic opportunities. *World J. Cardiol.* **10**, 74–86 (2018).
8. Pizzorno, J. Glutathione! *Integr. Med. Clin. J.* **13**, 8–12 (2014).
9. Bajic, V. P. *et al.* Glutathione "Redox Homeostasis" and Its Relation to Cardiovascular Disease. *Oxidative Medicine and Cellular Longevity* (2019) doi:10.1155/2019/5028181.
10. Shaw, J. P. & Chou, I.-N. Elevation of intracellular glutathione content associated with mitogenic stimulation of quiescent fibroblasts. *J. Cell. Physiol.* **129**, 193–198 (1986).
11. Zucker, B., Hanusch, J. & Bauer, G. Glutathione depletion in fibroblasts is the basis for apoptosis-induction by endogenous reactive oxygen species. *Cell Death Differ.* **4**, 388–395 (1997).
12. Markovic, J. *et al.* The Depletion of Nuclear Glutathione Impairs Cell Proliferation in 3t3 Fibroblasts. *PLOS ONE* **4**, e6413 (2009).
13. Kharb, S. Low blood glutathione levels in acute myocardial infarction. *Indian J. Med. Sci.* **57**, 335–337 (2003).
14. Shimizu, H. *et al.* Relationship between plasma glutathione levels and cardiovascular disease in a defined population: the Hisayama study. *Stroke* **35**, 2072–2077 (2004).
15. Damy, T. *et al.* Glutathione Deficiency in Cardiac Patients Is Related to the Functional Status and Structural Cardiac Abnormalities. *PLOS ONE* **4**, e4871 (2009).
16. Brown, D. A. *et al.* Cardiac Arrhythmias Induced by Glutathione Oxidation can be Inhibited by Preventing Mitochondrial Depolarization. *J. Mol. Cell. Cardiol.* **48**, 673–679 (2010).
17. Hayes, J. D., Flanagan, J. U. & Jowsey, I. R. Glutathione transferases. *Annu. Rev. Pharmacol. Toxicol.* **45**, 51–88 (2005).
18. Nebert, D. W. & Vasiliou, V. Analysis of the glutathione S-transferase (GST) gene family. *Hum. Genomics* **1**, 460–464 (2004).
19. Rinaldi, R., Eliasson, E., Swedmark, S. & Morgenstern, R. Reactive intermediates and the dynamics of glutathione transferases. *Drug Metab. Dispos. Biol. Fate Chem.* **30**, 1053–1058 (2002).
20. R Core Team. R: A language and environment for statistical computing. *R Found. Stat. Comput. Vienna Austria* (2019).
21. Carvalho, B. S. & Irizarry, R. A. A framework for oligonucleotide microarray preprocessing. *Bioinforma. Oxf. Engl.* **26**, 2363–2367 (2010).
22. MacDonald, J. W. clariomsmousetranscriptcluster.db: Affymetrix clariomsmouse annotation data (chip clariomsmousetranscriptcluster) (R package version 8.7.0). (2017).
23. Pagès, H., Carlson, M., Falcon, S. & Li, N. AnnotationDbi: Manipulation of SQLite-based annotations in Bioconductor (R package version 1.47.1). (2019).

24. Ritchie, M. E. *et al.* limma powers differential expression analyses for RNA-sequencing and microarray studies. *Nucleic Acids Res.* **43**, e47 (2015).
25. Warnes, G. R. *et al.* gplots: Various R Programming Tools for Plotting Data (R package version 3.0.1.1). (2015).
26. Chen, H. VennDiagram: Generate High-Resolution Venn and Euler Plots (R package version 1.6.20). (2018).
27. Wickham, H. ggplot2: Elegant Graphics for Data Analysis. *Springer-Verl. N. Y.* (2016).
28. Mi, H., Muruganujan, A., Ebert, D., Huang, X. & Thomas, P. D. PANTHER version 14: more genomes, a new PANTHER GO-slim and improvements in enrichment analysis tools. *Nucleic Acids Res.* **47**, D419–D426 (2019).
29. Fabregat, A. *et al.* The Reactome Pathway Knowledgebase. *Nucleic Acids Res.* **46**, D649–D655 (2018).
30. Schneider, C. A., Rasband, W. S. & Eliceiri, K. W. NIH Image to ImageJ: 25 years of image analysis. *Nat. Methods* **9**, 671–675 (2012).
31. Foth, C. & Mountfort, S. Acute Myocardial Infarction ST Elevation (STEMI). in *StatPearls* (StatPearls Publishing, 2019).
32. Thygesen Kristian *et al.* Third Universal Definition of Myocardial Infarction. *Circulation* **126**, 2020–2035 (2012).
33. Turillazzi, E., Di Paolo, M., Neri, M., Riezzo, I. & Fineschi, V. A theoretical timeline for myocardial infarction: immunohistochemical evaluation and western blot quantification for Interleukin-15 and Monocyte chemotactic protein-1 as very early markers. *J. Transl. Med.* **12**, 188 (2014).
34. Åström-Olsson, K. *et al.* Impact of hypoxia, simulated ischemia and reperfusion in HL-1 cells on the expression of FKBP12/FKBP12.6 and intracellular calcium dynamics. *Biochem. Biophys. Res. Commun.* **422**, 732–738 (2012).
35. Cicconi, S. *et al.* Characterization of apoptosis signal transduction pathways in HL-5 cardiomyocytes exposed to ischemia/reperfusion oxidative stress model. *J. Cell. Physiol.* **195**, 27–37 (2003).
36. Gille, J. J. P. & Joenje, H. Cell culture models for oxidative stress: superoxide and hydrogen peroxide versus normobaric hyperoxia. *Mutat. Res.* **275**, 405–414 (1992).
37. Anupama, V. *et al.* Molecular mechanisms in H2O2-induced increase in AT1 receptor gene expression in cardiac fibroblasts: A role for endogenously generated Angiotensin II. *J. Mol. Cell. Cardiol.* **97**, 295–305 (2016).
38. Mukhopadhyay, P., Rajesh, M., Yoshihiro, K., Haskó, G. & Pacher, P. Simple quantitative detection of mitochondrial superoxide production in live cells. *Biochem. Biophys. Res. Commun.* **358**, 203–208 (2007).
39. Majmundar, A. J., Wong, W. J. & Simon, M. C. Hypoxia-Inducible Factors and the Response to Hypoxic Stress. *Mol. Cell* **40**, 294–309 (2010).
40. Zhang, P., Su, J. & Mende, U. Cross talk between cardiac myocytes and fibroblasts: from multiscale investigative approaches to mechanisms and functional consequences. *Am. J. Physiol. Heart Circ. Physiol.* **303**, H1385-1396 (2012).
41. Lim, H.-Y., Wang, W., Chen, J., Ocorr, K. & Bodmer, R. ROS Regulate Cardiac Function via a Distinct Paracrine Mechanism. *Cell Rep.* **7**, 35–44 (2014).
42. Cartledge, J. E. *et al.* Functional crosstalk between cardiac fibroblasts and adult cardiomyocytes by soluble mediators. *Cardiovasc. Res.* **105**, 260–270 (2015).
43. Pellman, J., Zhang, J. & Sheikh, F. Myocyte-Fibroblast Communication in Cardiac Fibrosis and Arrhythmias: Mechanisms and Model Systems. *J. Mol. Cell. Cardiol.* **94**, 22–31 (2016).
44. Shi, H. *et al.* Metabolites of Hypoxic Cardiomyocytes Induce the Migration of Cardiac Fibroblasts. *Cell. Physiol. Biochem.* **41**, 413–421 (2017).

Supplementary Figures

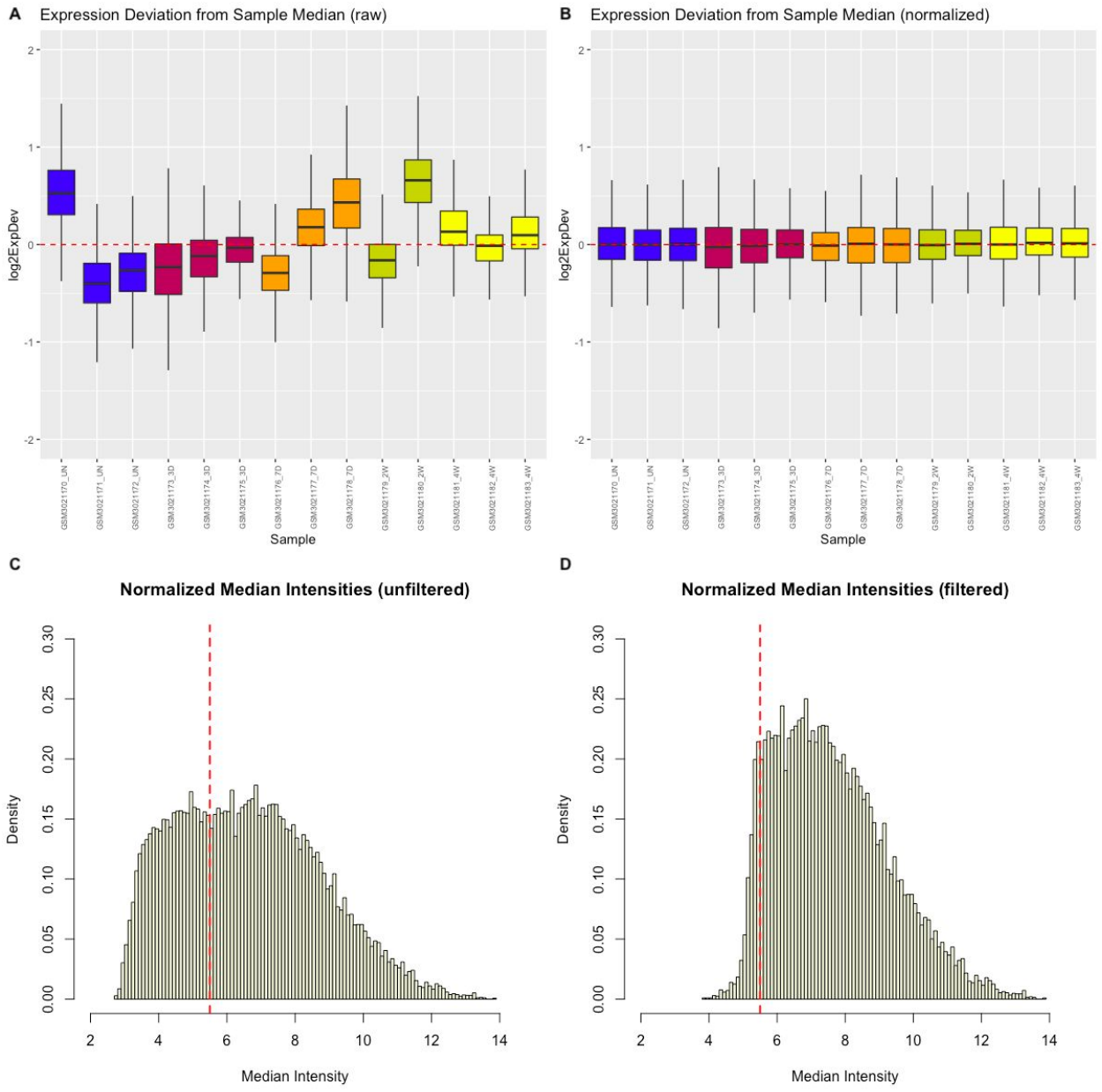

Figure S1. Quality control of data enables sample-to-sample comparison of transcriptionally-relevant genes. (**A**), (**B**) Raw fluorescence intensity values were processed using the Robust Multichip Average (RMA) quantile method in order to normalize genome-wide $\log_2$-expression deviation from each sample's median (dotted red line). (**C**), (**D**) Normalized fluorescence intensity values were subsequently filtered by excluding all transcripts which did not exceed the $\log_2$-intensity threshold value of 5.5 (dotted red lines) in at least 2 samples (corresponding to the smallest number of biological replicates across any timepoint), transforming the original bimodal distribution into a (right-skewed) unimodal distribution. Finally, only probe IDs corresponding to a single unique Official Gene Symbol ID were retained for analysis. Of the original cohort of 29,129 probe IDs, 8,375 were excluded based on the filtering threshold of 5.5, 4,412 were excluded for lacking an Official Gene Symbol ID, and 628 were excluded for mapping to more than one Official Gene Symbol ID, leaving a final total of 15,714 genes for downstream analysis.

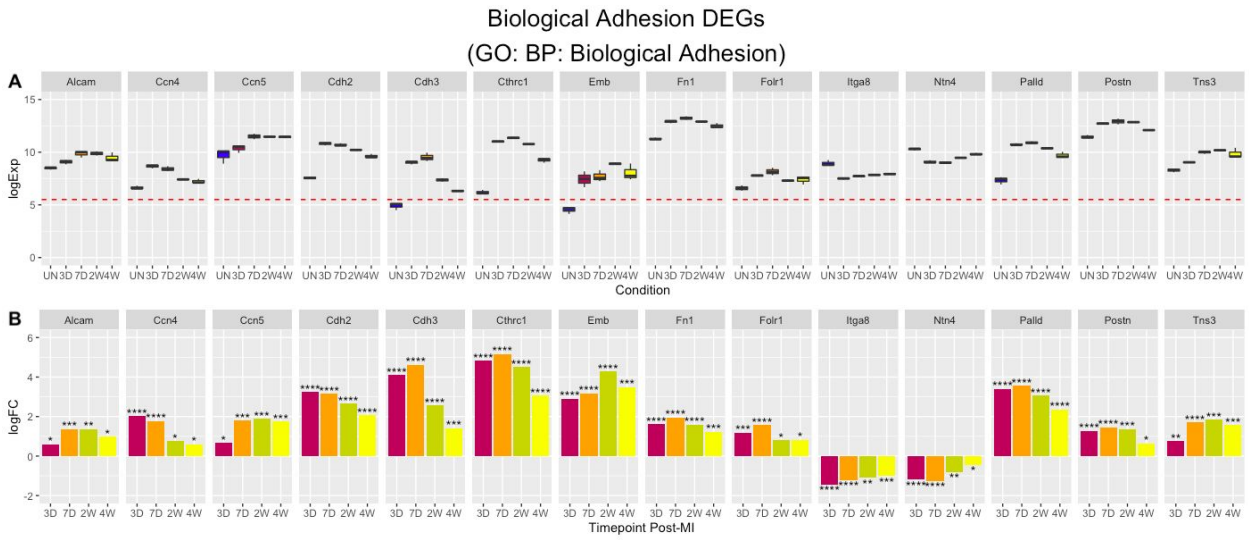

Figure S2. Numerous biological adhesion genes are primarily upregulated across the post-MI timecourse. (**A**) Log_2-expression of biological adhesion DEGs dysregulated across all post-MI timepoints. Dotted red line indicates median intensity threshold used to filter lowly-expressed probes (Figure S1). (**B**) Log_2-fold changes in expression for the same across all post-MI timepoints, relative to uninjured baseline. *p<0.05, **p<0.01, ***p<0.001, ****p<0.0001.

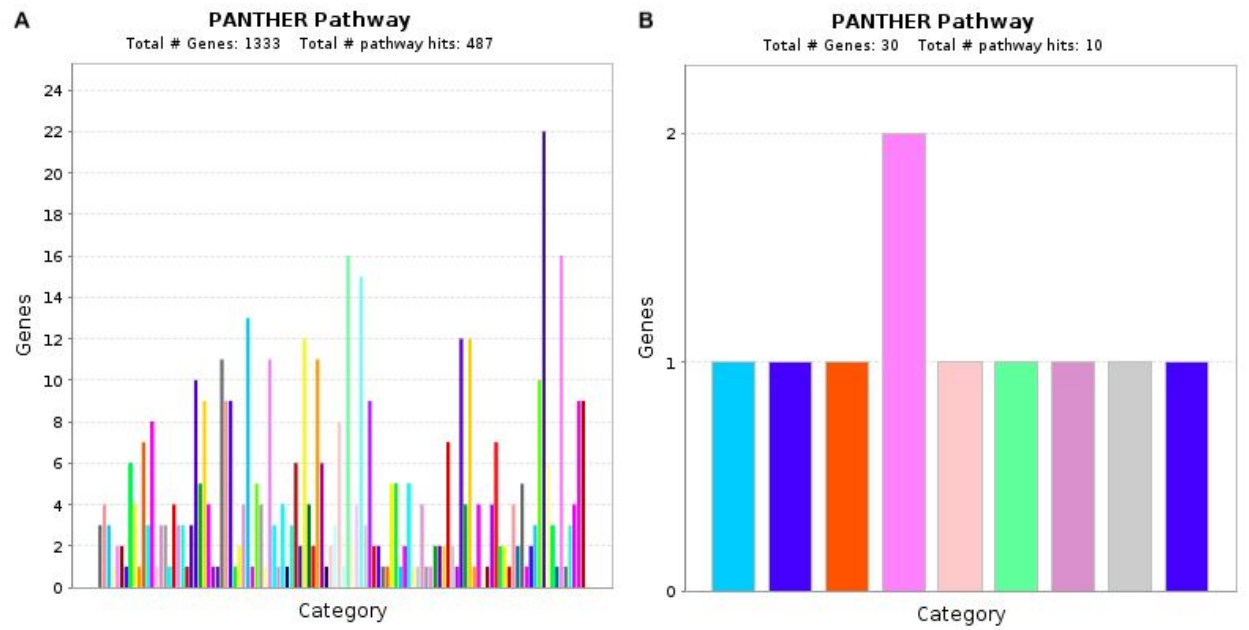

Figure S3. Inflammation and scarring pathways are upregulated in both acute and chronic phases post-MI. (**A**) PANTHER pathways represented by 1,333 DEGs significantly upregulated solely at 3D post-MI (58% of the 2,284 DEGs solely dysregulated at 3D post-MI (Figure 2B)). Top 4 pathways (left to right): chemokine/cytokine-mediated inflammation (green bar, 16 genes); integrin signaling (light blue bar, 15 genes); ubiquitin proteasome activity (purple bar, 22 genes); and Wnt signaling (pink bar, 16 genes). (**B**) PANTHER pathways represented by 30 DEGs significantly upregulated solely at 2W/4W post-MI (68% of the 44 DEGs solely dysregulated at 2W/4W post-MI (Figure 2B)). Selected pathways (left to right): angiogenesis (orange bar, 1 gene); fibroblast growth factor (FGF) signaling (pink bar, 2 genes); and chemokine/cytokine-mediated inflammation (green bar, 1 gene).

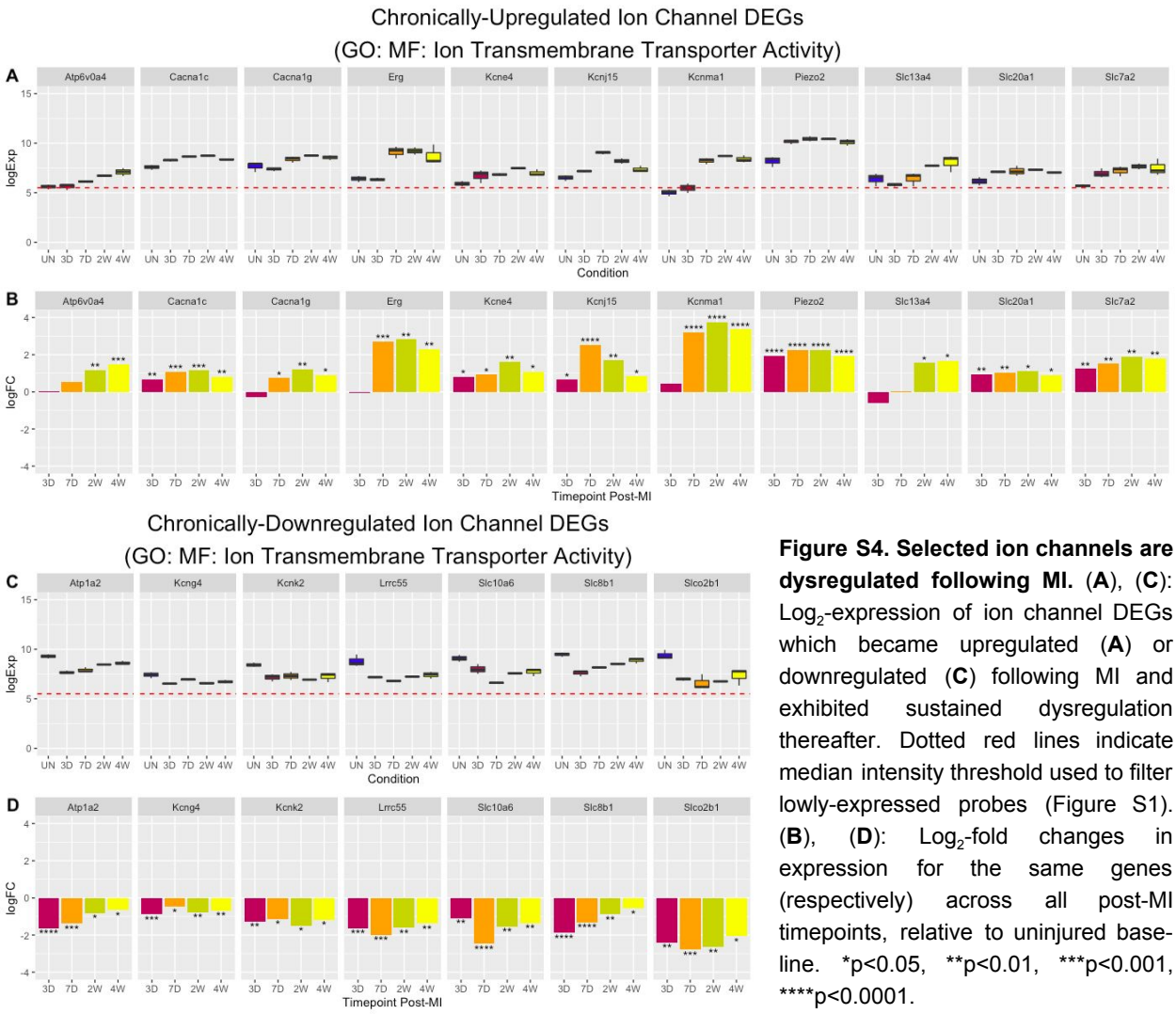

Figure S4. Selected ion channels are dysregulated following MI. (**A**), (**C**): Log_2-expression of ion channel DEGs which became upregulated (**A**) or downregulated (**C**) following MI and exhibited sustained dysregulation thereafter. Dotted red lines indicate median intensity threshold used to filter lowly-expressed probes (Figure S1). (**B**), (**D**): Log_2-fold changes in expression for the same genes (respectively) across all post-MI timepoints, relative to uninjured baseline. *p<0.05, **p<0.01, ***p<0.001, ****p<0.0001.

Figure S5. Glutathione-related genes merit further study in experimental MI/OS contexts. See Discussion for descriptions of genes. (**A**) Log_2-expression of glutathione-related DEGs of interest. Dotted red line indicates median intensity threshold used to filter lowly-expressed probes (Figure S1). (**B**) Log_2-fold changes in expression for the same genes across all post-MI timepoints, relative to uninjured baseline. *p<0.05, **p<0.01, ***p<0.001, ****p<0.0001.

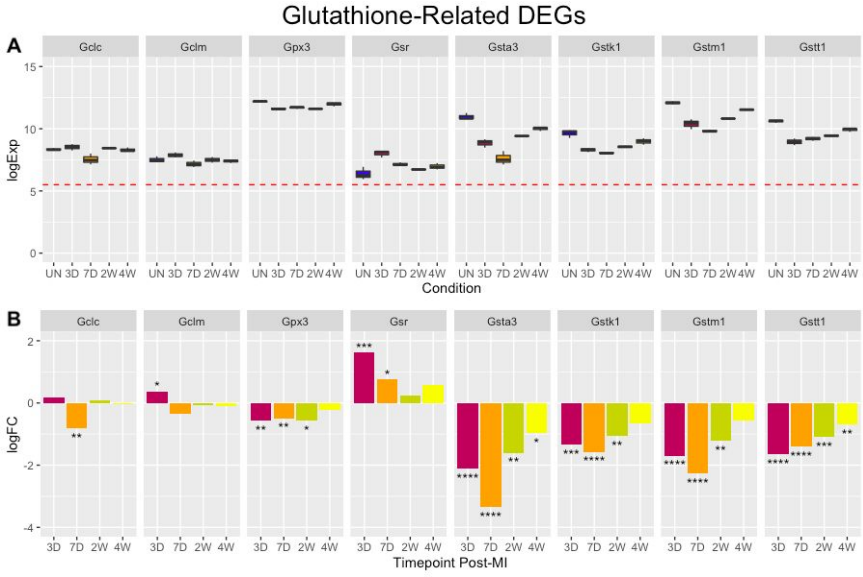

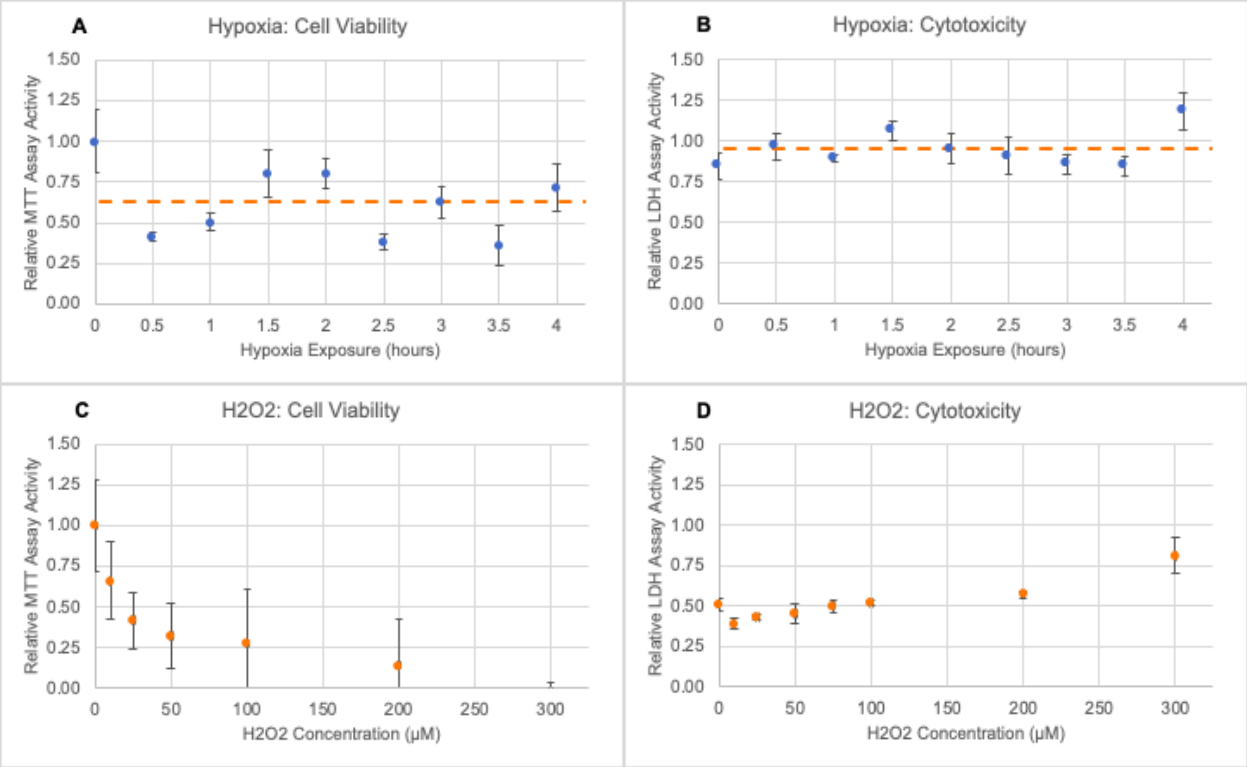

Figure S6. Moderate exposure to hypoxia or treatment with H_2O_2 diminishes cell viability and exerts mildly cytotoxic effects on hCFs. (**A**) Mean cell viability of P6 hCFs exposed to varying durations of hypoxia (3% O_2), as measured by MTT assay activity. (**B**) Cytotoxicity of the same conditions on the same cells, as measured by LDH assay activity. (**A**), (**B**): Dotted orange lines represent mean assay activities for cells exposed to hypoxia for 24 hours. (**C**) Mean cell viability of P6 hCFs exposed to varying concentrations of H_2O_2, as measured by MTT cell proliferation assay activity. (**D**) Cytotoxicity of the same conditions on the same cells, as measured by LDH assay activity. Error bars represent mean values ± SEM for all cells and conditions (n = 2–3 biological replicates per condition).

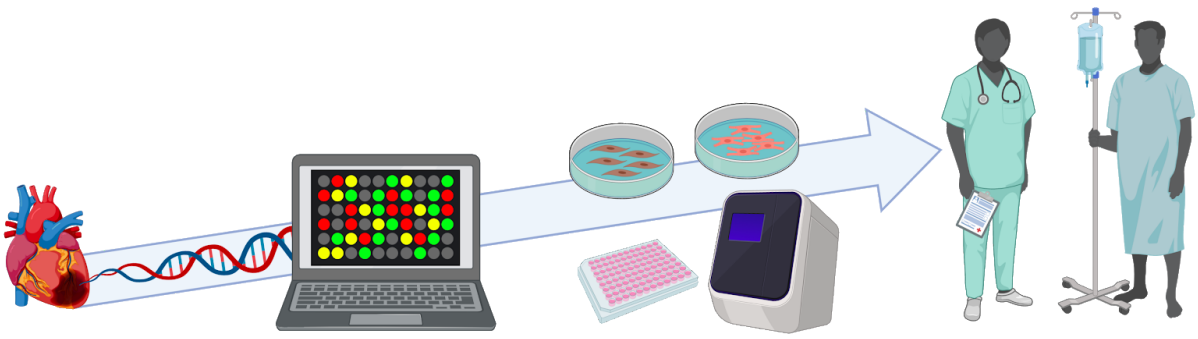

Figure S7. From Bioinformatics and the Bench to the Bedside. Schematic of the translational research approach taken here to identify novel gene pathways for combating post-infarction dysregulation of cardiac gene expression (image credits: BioRender).